Cement & Concrete Composites 37 (2013) 276–292

Contents lists available at SciVerse ScienceDirect

Cement & Concrete Composites

journal homepage: www.elsevier.com/locate/cemconcomp

# Properties of interfacial transition zones in recycled aggregate concrete tested by nanoindentation

Jianzhuang Xiao [a,*], Wengui Li [a,b], Zhihui Sun [c], David A. Lange [d], Surendra P. Shah [b]

[a] Department of Building Engineering, Tongji University, Shanghai 200092, PR China
[b] Center for Advanced Cement-Based Materials, Northwestern University, Evanston, IL 60208, United States
[c] Department of Civil & Environmental Engineering, University of Louisville, Louisville, KY 40292, United States
[d] Department of Civil & Environmental Engineering, University of Illinois at Urbana-Champaign, Urbana, IL 61801, United States

ARTICLE INFO

*Article history:*
Received 6 July 2012
Received in revised form 27 October 2012
Accepted 11 January 2013
Available online 22 January 2013

*Keywords:*
Recycled Aggregate Concrete (RAC)
Interfacial Transition Zone (ITZ)
Atomic Force Microscope (AFM)
Nanoindentation
Nanomechanical properties
Microstructure

ABSTRACT

The properties of new Interfacial Transition Zone (ITZ) and old ITZ in Recycled Aggregate Concrete (RAC) were investigated by Atomic Force Microscopy (AFM), Scanning Electron Microscopy (SEM) and nanoindentation. From the SEM images, obvious voids and high concentration of calcium hydroxide can be found in both old ITZ and new ITZ in RAC. Based on the nanoindentation study, it is indicated that the thicknesses of old and new ITZs are in the range 40–50 μm and in the range 55–65 μm, respectively. It is also found that the average indentation modulus of old ITZ is 70–80% of that of old paste matrix, while the average indentation modulus of new ITZ is 80–90% of that of new paste matrix. Additionally, the influences of mix proportion, aggregate types and hydration age on the properties of ITZs in RAC are discussed in this study.



## 1. Introduction

Recycling of waste concrete is necessary from the viewpoints of environmental preservation and effective utilization of resources. Recycled Aggregate Concrete (RAC) usually either fully or partially uses crushed and sieved waste concrete as its coarse aggregates [1–4]. Researches based on the comparisons of workability, mechanical properties, and shrinkage and creep with respect to conventional concrete have been published to investigate the early and long-term behaviors of RAC [5–10]. However, very limited studies have been reported to investigate the microstructure of RAC and its effect on the mechanical properties [11,12]. As already known, two types of interfaces exist in RAC: the old Interfacial Transition Zones (ITZs) between adhered old cement mortar and natural aggregates, and the new ITZs between new cement mortar and the aggregates (either recycled aggregates or natural aggregates). This is one of the main differences between RAC and conventional concrete. It is widely accepted that the ITZs in RAC have significant influences on the mechanical properties. Ryu found that the failure behaviors of the RAC depended on the relative quality of old ITZ and new ITZ [13]. The strength of the RAC depends on the quality of new ITZ when the quality of old ITZ is better than that of new ITZ. Otherwise, the strength of RAC depends on the quality of old ITZ. To investigate the effect of the recycling process on recycled aggregate, Nagataki et al. concluded that recycling processing level and quality of the waste concrete played a very important role in the characteristics of recycled aggregates [14].

In the past, researchers expressed considerable interests in the micromechanical properties of old and new ITZs in RAC to help understanding the complex mechanical behaviors of RAC such as failure mechanism and durability [5,13–15]. However, due to the difficulties in determining constitutive parameters with the available testing methods, the understanding of the fundamental properties of the ITZs in RAC on submicron or nanoscales is still very limited. With the emergence of nanoindentation technology, it is now possible to directly measure the nanomechanical properties of the thin ITZs [16–18]. The nanoindentation technique is similar to classical indentation, but is capable of producing contact areas and penetration depths on submicron or nanoscales for cementitious materials [19–22]. In nanoindentation tests, the contact area is measured directly from the depth of penetration of the indenter into the specimen surface and the geometry of the indenter [23,24]. Atomic Force Microscopy (AFM) is another increasingly popular tool for studying cement-based materials [25,26], which is often used to assess concrete surface roughness. In order to study the microstructural gradients of the ITZ in concrete, Scanning

* Corresponding author. Tel.: +86 21 65982787; fax: +86 21 65986345.
*E-mail address:* jzx@tongji.edu.cn (J. Xiao).

0958-9465/$ - see front matter © 2013 Elsevier Ltd. All rights reserved.
http://dx.doi.org/10.1016/j.cemconcomp.2013.01.006


**Fig. 1.** Recycled coarse aggregate (4.75–25.0 mm) (Rossi Contractors Inc. in Chicago, IL).

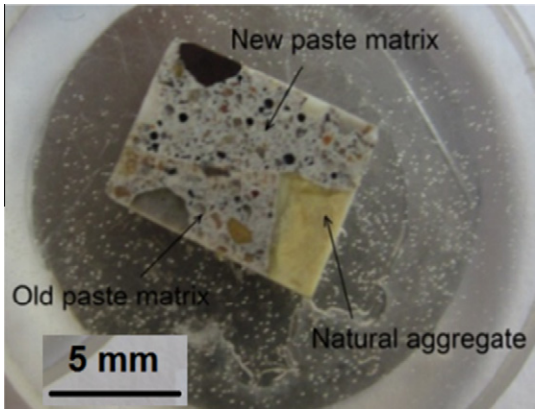


**Fig. 2.** RAC sample after grinding and polishing.

Electron Microscopy (SEM) is usually applied [27,28]. With SEM technique, one can identify the phase distribution, such as C–S–H or CH, in concrete.

To understand the influence of ITZ properties on RAC properties, the first step is to study how the ITZ properties change when subjected to various influencing factors. Because ITZ is a layer formed between an aggregate and the paste matrix, its properties are affected by both of them. It was found that the cementitious materials grain size distribution, water-to-binder ratio, hydration age, mixing approach, aggregate size, and aggregate type, etc. have effects on the ITZ properties [29–32]. For example, it was found that the thickness of ITZ increases with increasing water-to-binder ratio (w/b) and aggregate size. Moreover, the composition and particle size distribution of the binder can also affect the porosity of the ITZ [33]. Finer particles, such as silica fume, can decrease ITZ porosity and the thickness [34]. Researchers also found that the size and surface texture of the aggregates have great influences on ITZ properties. Compared with gravel, a limestone is more porous and has a rough surface texture. Therefore, the ITZ around a limestone can be relatively stronger and thinner [31]. In order to investigate both the micromechanical properties and phase distributions on micron and submicron scales, this paper utilizes the introduced three advanced techniques (nanoindentation, AFM, and SEM) to study the influences of mix proportion, aggregate type and hydration age on the properties of old and new ITZs mainly including their elastic moduli and thicknesses.

## 2. Research scope and significance

This research mainly focuses on studying two properties of ITZs: the elastic modulus and the thickness. Knowing the elastic modulus distribution within ITZs can help to improve our knowledge of the failure mechanism and cracking progresses in RAC. And knowing the thickness can help to develop methodologies to improve the quality of RAC by minimizing the ITZ volume.

The objective of this study is to investigate the influences of mix proportion and hydration ages on the characteristics (modulus and thickness) of ITZs in RAC by three testing methods: nanoindentation, AFM, and SEM. This study presents two gaps in the current understanding of RAC behavior by: (1) obtaining a more accurate understanding of local mechanical properties on nanoscales for ITZs in RAC and (2) revealing the differences in nanoscale mechanical properties between old and new ITZs in RAC. The experimental results of this work should be beneficial for future studies to correlate the microstructure and nanomechancial properties to the macroscopic mechanical behaviors of RAC.

## 3. Materials and methods

### 3.1. Materials and mixing approach

Recycled aggregates (as shown in Fig. 1) from Rossi Contractors Inc. at the Chicago O'Hare International Airport were used to prepare RACs in this study. The specific gravity and the water absorption capacity of these recycled aggregates were 2.41 and 5.51%, respectively. Most of natural aggregates in the recycled coarse aggregate were limestone, except a few of them were gravel. Due to the high water absorption, the RCAs used for casting RAC specimens were presoaked before mixing. The water amount used to presoak the RCA was calculated according to the water absorption capacity of RCA. The maximum size of coarse aggregates was about 20 mm. Two different RACs were mixed and investigated in this study (Table 1). One was prepared with a water-to-binder ratio (w/b) of 0.42 (noted as RAC I). The Type I Portland cement content was 246 kg/m$^3$and the Class C fly ash content was 61 kg/m$^3$ in RAC I. The other RAC used in this study had a water-to-cement ratio (w/c) of 0.45, where the Type I Portland cement, water, and river sand were applied (noted as RAC II). Compared to RAC I, no fly ash was used in RAC II mixture. For both mixtures, a Two-Stage Mixing Approach (TSMA) was applied when preparing the RAC specimens [35]. During mixing, the required water was proportionally split into two parts that were added at different timing. All of the samples were cured under 25 °C and 55% relative

**Table 1**
Mix proportions of RAC I and RAC II.

| | w/b (w/c) | kg/m$^3$ | | | | | Mixing approach |
|---|---|---|---|---|---|---|---|
| | | Water | Cement | Fly ash | Sand | Recycled coarse aggregate | |
| RAC I | 0.42 | 129 | 246 | 61 | 854 | 978 | TSMA |
| RAC II | 0.45 | 200 | 444 | 0 | 702 | 1054 | TSMA |

*Note*: TSMA means two-stage mixing approach.

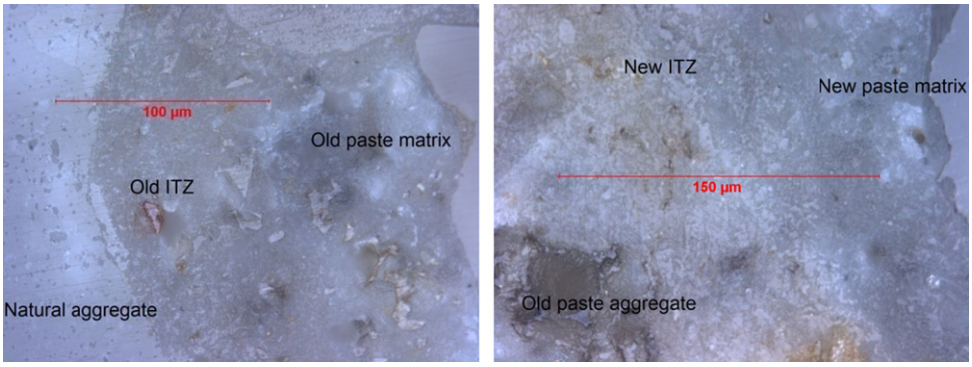


(a) Old ITZ (b) New ITZ

**Fig. 3.** Optical microscopy images of RAC ITZs after polishing.

**Table 2**
RMS roughness measurement for interfaces in RAC I.

| Scanning location | Scanning size (μm) | Average RMS roughness (nm) | RMS roughness deviation (nm) |
|---|---|---|---|
| Old ITZ | 50 × 50 | 97.2 | 25.3 |
| New ITZ | 50 × 50 | 90.2 | 21.6 |

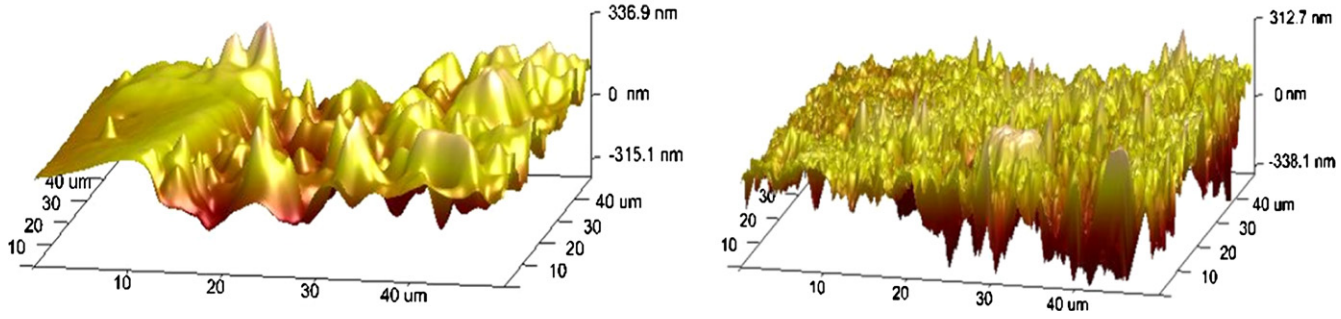


(a) Old ITZ (50×50μm) (b) New ITZ (50×50μm)

**Fig. 4.** Typical AFM 3D topography image of ITZs in RAC.

humidity laboratory conditions for 7, 28 and 90 days until the day of testing.

In this paper, the old ITZ represents the interfaces between the natural aggregate and old paste matrix in original crushed concrete; and the new ITZs are those interfaces around recycled aggregates (here, are the aggregates consists of old cement paste in particular) in newly cast concrete. Therefore, the recycled aggregate is termed as old paste aggregate in the following discussions.

### 3.2. Sample preparation

For nanoindentation test, 20 mm thick RAC slices were first cut from RAC prisms. The 20 mm thick slices were then cut into approximate 5 mm thick slices of 10 × 5 mm (cross section) with a diamond saw. The cut slices were immersed in ethanol for 24 h. The slices were then removed from the ethanol and were subjected to a heat treatment (drying) of 50 °C for 12 h. Since the microstructure of cementitious materials can easily be damaged by grinding and polishing, it is essential to fill the pores of the sample with epoxy resin impregnation prior to grinding and polishing. When the epoxy gets hardened, it stabilizes the microstructure and enables it to withstand the stresses of grinding and polishing without any alternations [36]. For the impregnation, the concrete slice was first placed in a 38.1 mm diameter blue rubber mold. Epoxy called Struers provided by Cytec Industries Inc. was then used. The vacuum to the chamber was then released, allowing atmospheric pressure to facilitate impregnation. The mold was then removed from the vacuum chamber and cured for 12 h in an oven at 70 °C.

The biggest challenge and critical step in preparing RAC slices for nanoindentation is to polish the sample to provide a smooth and flat surface, while minimizing the sample disturbance [16,18,19,25]. To ensure the reproducibility of the small penetration of the indenter, special attention needs be paid to the quality of the polished sample surface so that the elastic modulus and the hardness can be measured with nanoindentation. In this study, the sample was mounted on a metal holder using adhesive for grinding and polishing. And the sample holder was always placed within an annular metal collar. This configuration prevented any wobbling of the sample holder and helped to maintain parallel top and bottom surfaces while grinding and polishing.

There are three primary goals for surface grinding and polishing: (1) to achieve surfaces as flat as possible, (2) to obtain repeatable results, and (3) to minimize the sample disturbance. The procedure described here was optimized to satisfy these goals:

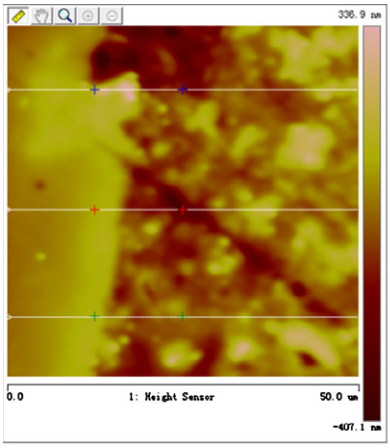


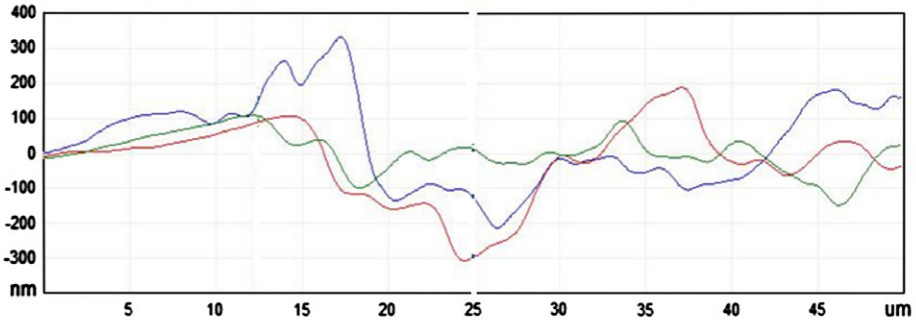


(a) Old ITZ region

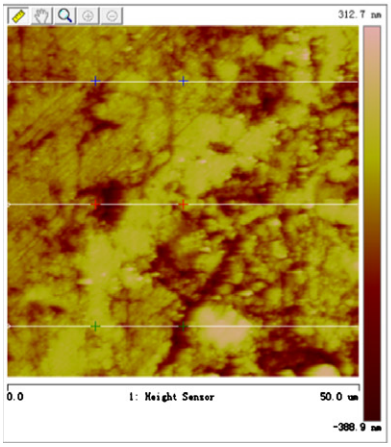


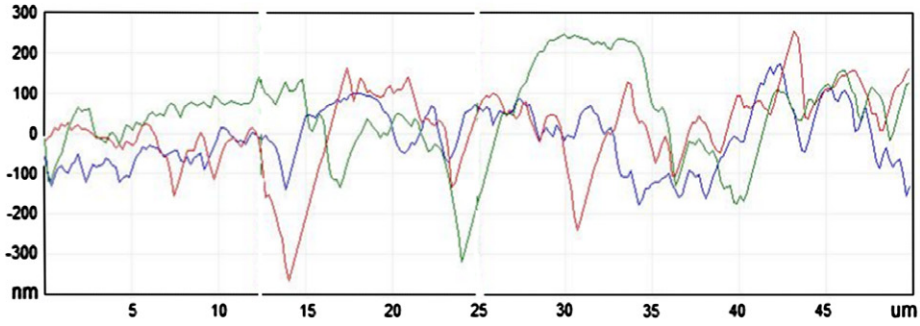


(b) New ITZ region

**Fig. 5.** Typical surface topography of RAC ITZs by AFM.

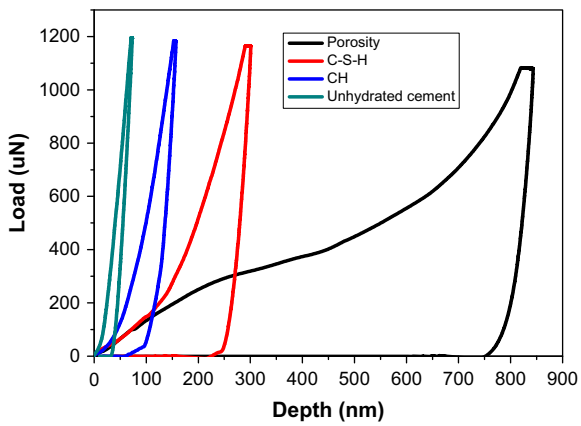


(a) Load-depth diagrams of different phases

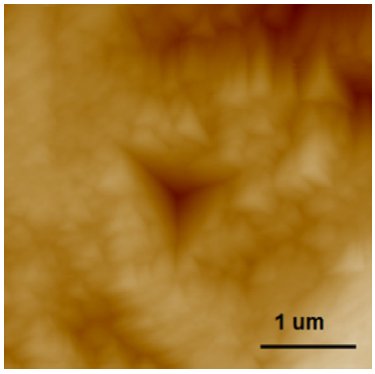


(b) Indent mark on C-S-H

**Fig. 6.** Typical indentation in ITZs of RAC.

- The sample was initially ground on Buehler-Met II paper disks with gradation of grits 280 (51.8 μm), 800 (22.1 μm), 1200 (14.5 μm) and 1500 (12.2 μm), respectively. Water was used as the cooling medium and lubricant. Approximate grinding time on each gradation was 5 min. The sample was then cleaned in ethanol in an ultrasonic cleaner before further polishing.
- After much trial and error with a variety of polishing compounds and polishing mats, one combination can provide a repeated success by lengthy polishing under light load. An auto-polisher was used with diamond suspensions in ethanol with gradation of 9 μm, 6 μm and 3 μm. The relatively slow lapping speed minimized the sample disturbance and created a

smooth surface. Each step lasted approximately 30 min. In the following steps, diamond lapping films from Allied High Tech Products Inc. with gradations of 3 μm, 1 μm and 0.5 μm were used. The hardness of diamond lapping film can assure that the higher surfaces of the sample are removed first, and the perforation gives a place for the polishing residue to collect without interfering with the polishing itself. In these steps, manual and semi-automated polishing was used. The ethanol was used as the cooling medium, and each polishing step lasted approximate 30 min.

- An ultrasonic bath cleaning in ethanol was performed for 10 min to remove all dust and diamond particles. After polishing, the surface quality was confirmed using a microscope, and then the sample was stored in a small air-tight container (Fig. 2).

The degree to which the RAC can be polished for nanoindentation studies is associated with the microstructure heterogeneity. On the micro-scale, RAC is composed of several relatively hard phases (natural aggregate, quartz and unhydrated cement particles) surround by old paste matrix and new paste matrix. At higher magnification, many different phases of RAC can be observed by optical microscopy (Fig. 3).

### 3.3. Atomic force microscopy

In order to guarantee the surface quality of polishing and grinding, the polished samples were further evaluated by AFM (Bruker AXS Dimension ICON) to obtain the surface topographic information. In AFM, a silicon tip was used with a cantilever arm. All the samples were scanned by using the tapping mode to obtain a topographic map around the interfaces in RAC, and the scanning was performed with an amplitude set point of 250 mV and a scan rate of 0.75 Hz. The scan was concentrated to observe a region of the paste matrix at the interfaces in RAC. The scanning sizes performed at both old and new ITZs were 50 × 50 μm. A total of 10 scans were conducted for each kind of ITZ. The results presented in this paper consisted of typical results obtained from these AFM scans, such as the surface topography and quantitative roughness. The Root-Mean-Squared (RMS) average of the topography of the surface was chosen to measure the surface roughness.

Following the AFM imaging procedure, each image was digitally analyzed in order to extract a roughness value. Before calculating the roughness, a linear slop correction was performed to account for an alignment difference between the reference plan of AFM imaging and the overall slope of the sample surface. The preferred parameter for roughness was a RMS average of the topography of the surface ($R_q$). The average RMS values of 10 scans at each location (old ITZ and new ITZ) of the sample are given in Table 2.

The AFM results of roughness at different locations suggest roughness measurement exhibit variation. A possible explanation for this variation is that the polished surface is inherently heterogeneous. The old ITZs exhibited higher roughness than that of the new ITZs. A comparison of the 3D topography images obtained by the AFM at old and new ITZs is presented in Fig. 4. In the figures, the bright areas represent the natural aggregate or unhydrated cement particles, while the dark areas are considered to be the pores and cracks. Fig. 5 shows the comparison of old ITZ and new ITZ cross-section height distribution (surface topography) along different sections. According to the three height distribution curves, it can be found that both the old ITZ and new ITZ regions are relatively flat in RAC.

## 4. Nanoindentation investigation

### 4.1. Nanoindentation details

Hysitron Triboindenter fitted with a Berkovitch tip (tip radius of 0.6 μm, angle of 142.3°) was used to determine the nanomechanical properties of the ITZs in RAC. A quartz standard was indented during each test to ensure accuracy. To account for possible surface roughness, head repositioning was carried out before each indent.

Researchers have shown that the indentation depth should be larger than the RMS of roughness, but how much larger remains an open argument for cement-based materials [18,25]. In this study, the nanoindentation was performed to an average depth of 350 nm for the ITZ phase with a sufficient surface roughness lower than 100 nm. The average indentation depth which is 3 times more than surface roughness should be sufficient to avoid effects of roughness. Each load/displacement diagram was plotted and inspected for signs of problems due to surface roughness, such as abnormal or discontinuous shapes. Fig. 6 presents load-depth curves of different phase in ITZ and the image of indent mark on the calcium silicate hydrate (C–H–S) gel after nanoindentation captured with indenter tip of the Triboindenter. The trapezoidal load functions which included single-cycle and multiple-cycle loads were used in this study. It is found that multiple cycles of partial loading and unloading lead to minimizing of the short-term creep and size effect [37].

All tests were programmed in a multi-cycle loading way that the indenter came into contact with the sample surface with the

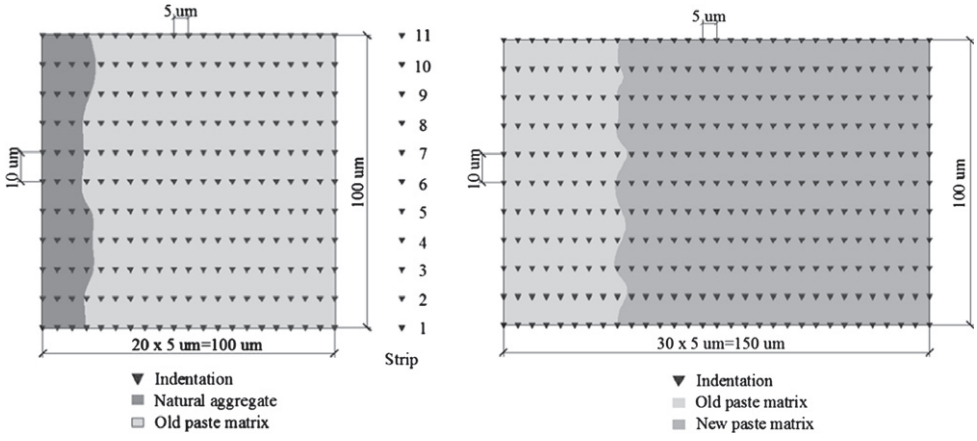


(a) Across old ITZ (b) Across new ITZ

**Fig. 7.** Schematic showing indented area of old ITZ and new ITZ in RAC.

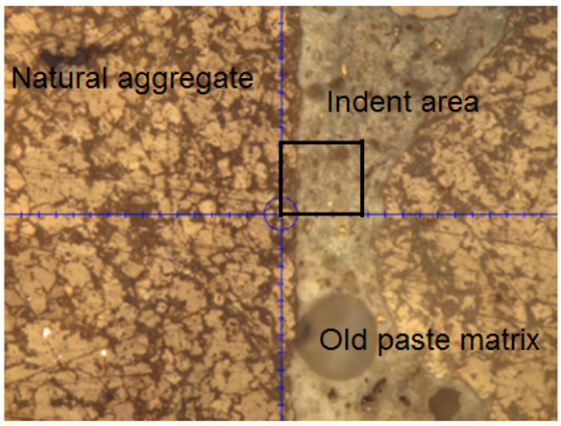


(a) Old ITZ, indent area:100×100μm

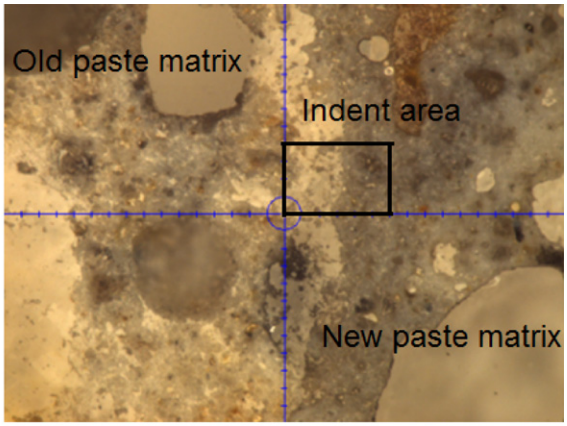


(b) New ITZ, indent area:150×100μm

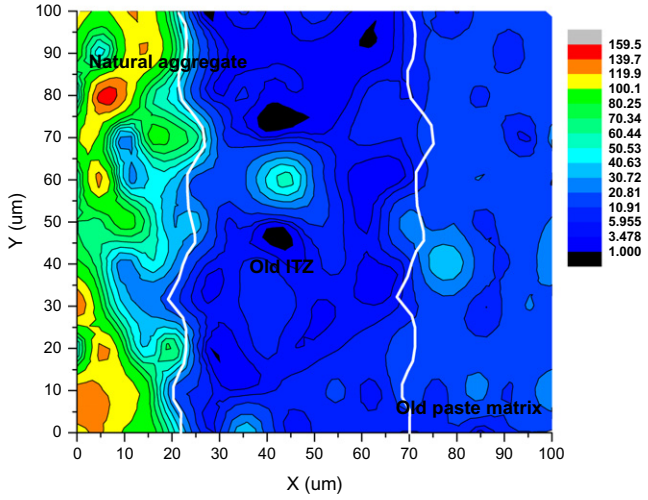


(c) Contour map of modulus in GPa (old ITZ)

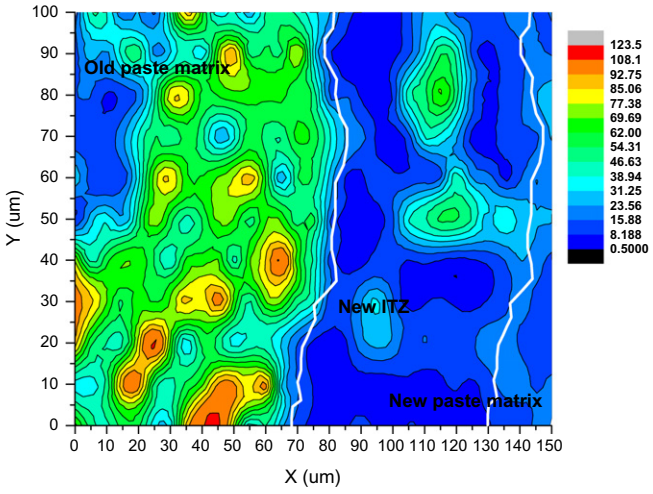


(d) Contour map of modulus in GPa (new ITZ)

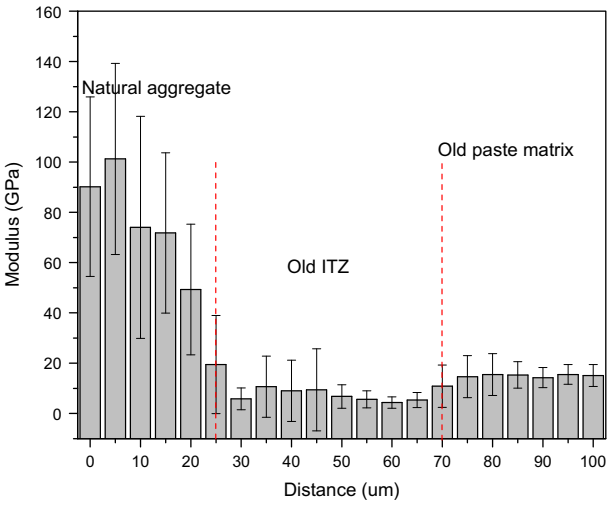


(e) Modulus distribution across old ITZ

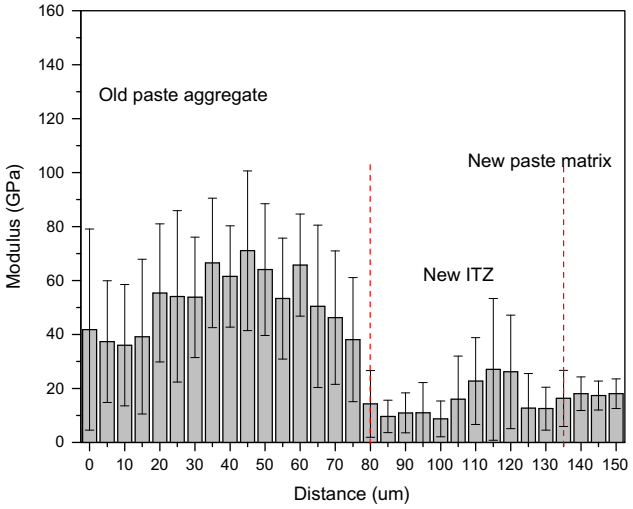


(f) Modulus distribution across new ITZ

**Fig. 8.** Grid indentation modulus on ITZs of RAC I at 90 days.

load increased at a constant rate of 120 μN and the maximum load was 1200 μN. Normally, grid indentation is a method to perform large number of indents on the sample. Statistical analysis of these data obtained from grid indentation provides information about the overall nanomechanical properties of the sample and volume fractions of different phases involved. In this study, indentation with in situ imaging was used to determine the local nanomechanical properties at specific locations of the sample.

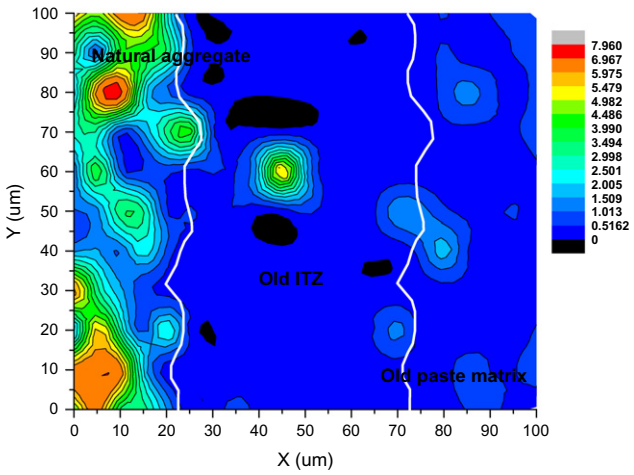


(a) Contour map of hardness in GPa (old ITZ)

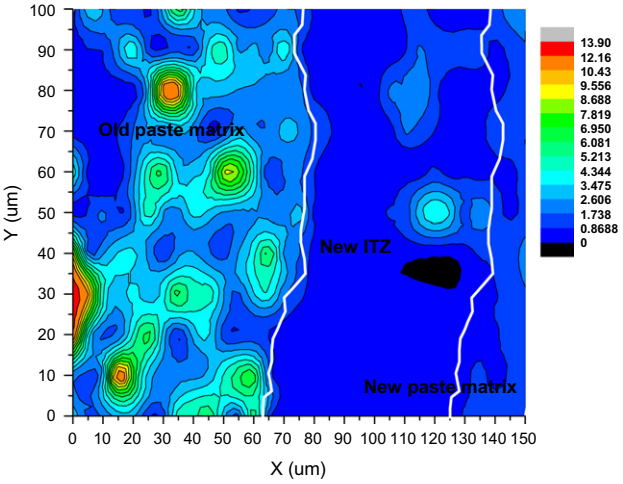


(b) Contour map of hardness in GPa (new ITZ)

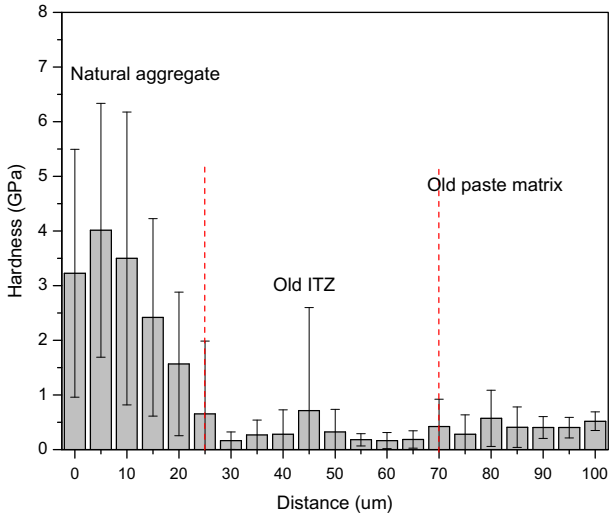


(c) Hardness distribution across old ITZ

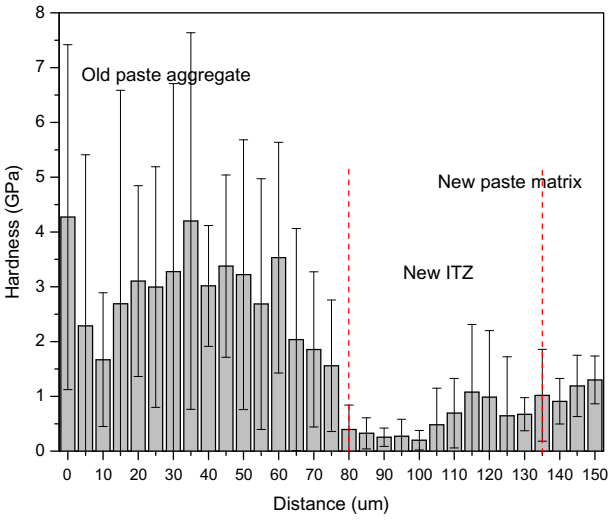


(d) Hardness distribution across new ITZ

**Fig. 9.** Grid indentation hardness on ITZs of RAC I at 90 days.

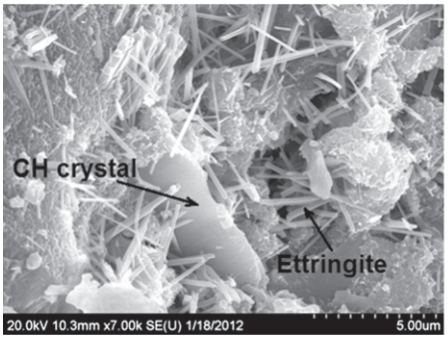


(a) Perpendicular to old ITZ, at old paste matrix side

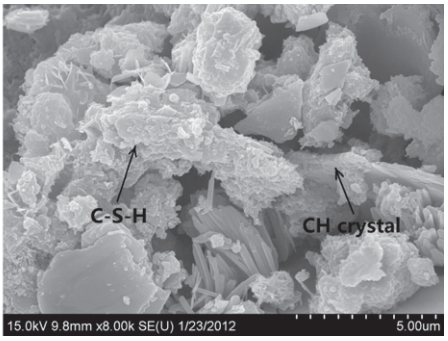


(b) Perpendicular to new ITZ, at new paste matrix side

**Fig. 10.** SEM images of old ITZ and new ITZ in RAC at 90 days.

A typical indentation load and indentation displacement curve includes peak indentation load ($P_{max}$), indentation depth at peak load ($h_{max}$), and final depth of the contact impression after unloading ($h_f$). As to the penetration of elastic half space by an axisymmetric indenter of arbitrary smooth profile, by applying a continuum scale model, the initial unloading stiffness $S = dp/dh$, is given as follows [16,23]:

$$S = \frac{dp}{dh} = \frac{2}{\sqrt{\pi}} E_r \sqrt{A} \tag{1}$$

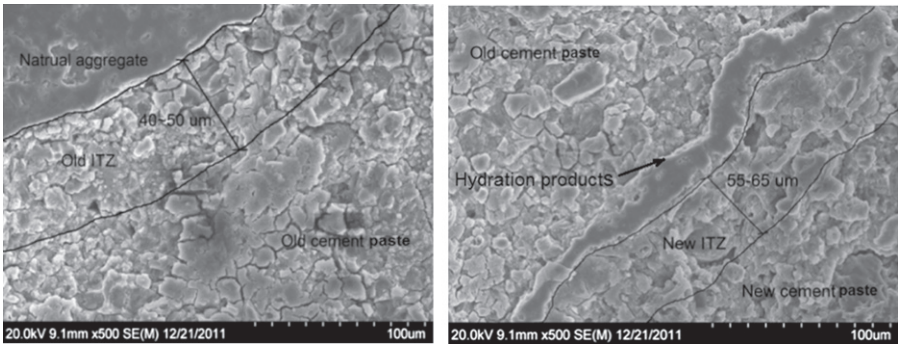


(a) old ITZ (b) new ITZ

**Fig. 11.** SEM images of polished new ITZ and old ITZ of RAC at 90 days.

where $A$ is the projected contact area at the peak load; $E_r$ is the reduced elastic modulus, which can be determined by nanoindentation. The relationship between $E_r$ and $E_i$ can be given by:

$$\frac{1}{E_r} = \frac{(1-v^2)}{E} + \frac{(1-v_i^2)}{E_i} \tag{2}$$

where $E$ and $v$ are Young's modulus and Poisson's ratio of the sample respectively, and $E_i$ and $v_i$ are the corresponding parameters of the indenter. For the indenter used in the present experiment, the elastic modulus $E_i$ = 1140 GPa and the Poisson's ratio $v_i$ = 0.07. Then, the elastic modulus $E$ of the sample can be calculated by:

$$E = (1-v^2) \times \left[\frac{1}{E_r} - \frac{(1-v_i^2)}{E_i}\right]^{-1}. \tag{3}$$

The suggested Poisson's ratio for RAC is $v$ = 0.2, which was used in this study to calculate $E$ in Eq. (3) [16,23].

The hardness $H$ has the definition as follows:

$$H = \frac{P_{\max}}{A} \tag{4}$$

The studied areas were taken randomly within old ITZs and new ITZs in RAC that were around aggregates with similar sizes. The spacing between the indents was 5 μm and 10 μm in the lateral and vertical directions, respectively. The indent areas for old and new ITZs had the dimensions of $100 \times 100$ μm and $150 \times 100$ μm, respectively, as shown in Fig. 7. As for the old ITZs, 231 indents were made in an array at each studied area. For new ITZs, 341 indents were made in an array. For each old and new ITZ, four studied areas across interfaces were randomly chosen for nanoindentation. These four indented areas obtained for ITZs were based on the statistical consideration, which was used to calculate the mean and standard deviation values for the nanomechanical properties of ITZs. As the spacing between indents was 5 μm in lateral direction, the strips of 5 μm wide were successively taken from the indented areas in RAC. For each trip, 11 indentation values with 10 μm spacing in one trip were then averaged. The distributions of nanomechanical properties were obtained with the distance starting at natural aggregate surrounded by old ITZ or old paste aggregate surrounded by new ITZ. In this study, the distributions of indentation modulus were used as a basis for the characterizations of old ITZ and new ITZ respectively, such as ITZ thickness.

### 4.2. Grid nanoindentation

For the RAC I samples at 90 days, areas on the samples that contained old and new ITZs were chosen for indentation (Fig. 8a and b). The ITZs around coarse limestone aggregates with around 20 mm size were chosen for indentation. Fig. 8c and d shows the contour maps of indentation modulus of old and new ITZs, respectively. The deep blue[1] and black areas have the lowest moduli, which indicate relatively weaker zones in the RAC. The results also show that these blue and black areas are distributed in the regions between natural aggregates and old paste matrix, as well as between old paste matrix and new paste matrix. This is an important indication of the existence of old ITZ and new ITZ in RAC.

Fig. 8e and f shows the indentation modulus distributions with the distances across old ITZ and new ITZ, respectively. According to other researchers [19,38], the indentation modulus of calcium hydroxide (CH) is higher than that of calcium silicate hydrate (C–S–H). The porosity and CH can be concentrated when approaching the aggregate surface and old paste matrix in both old and new ITZs due to the wall effect.

In this study, the ITZ thickness was estimated by locating the place where there is little variation in indentation modulus with the distance from the natural aggregate (for old ITZ) or old paste aggregate surface (for new ITZ), and the indentation modulus distribution of ITZ seems to become close to those of the paste matrix. For the old ITZ, the thickness of the interfacial zone ranges between 40 μm and 50 μm. This supports the ITZ thickness of conventional concrete previously found by other researchers to be from 20 μm to 50 μm by analyzing the lateral variation in properties around aggregate [29–32,39]. The average modulus of the old ITZ was found to be 70–80% of that of the old paste matrix. However, the indentation modulus values obtained around the aggregate does not increase consistently when moving away from the aggregate surface and the ITZ modulus is not necessary always lower than that of the paste matrix. This phenomenon may be due to the concentration of porosity and CH crystals in the interfacial zone.

For the new ITZ, the thickness was estimated to be in the range of 55–65 μm, which was greater than that of old ITZ. Moreover, the average indentation modulus of new ITZs was found to be approximately 80–90% of that of the new paste matrix. Similar to the old ITZ, there is no obvious trend for the modulus of new ITZ to increase with an increasing distance from the old paste aggregate surface. However, the indentation modulus of new ITZ appears to be higher than that of old ITZ in RAC. This may be because the improved mixing method TSMA coats the recycled aggregate with cement, and further hydration takes place between old paste matrix and new paste matrix.

Fig. 9a and b shows the contour map of indentation hardness of the old and new ITZs in RAC I. It is found that the characterization of indentation hardness distribution was close to that of indentation

[1] For interpretation of color in Figs. 8 and 12, the reader is referred to the web version of this article.

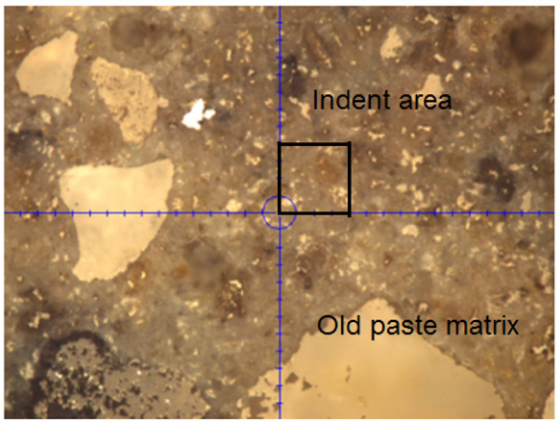


(a) Old paste matrix:100×100μm

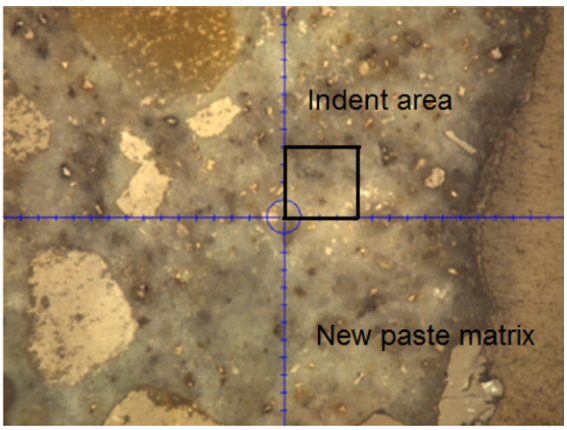


(b) New paste matrix:100×100μm

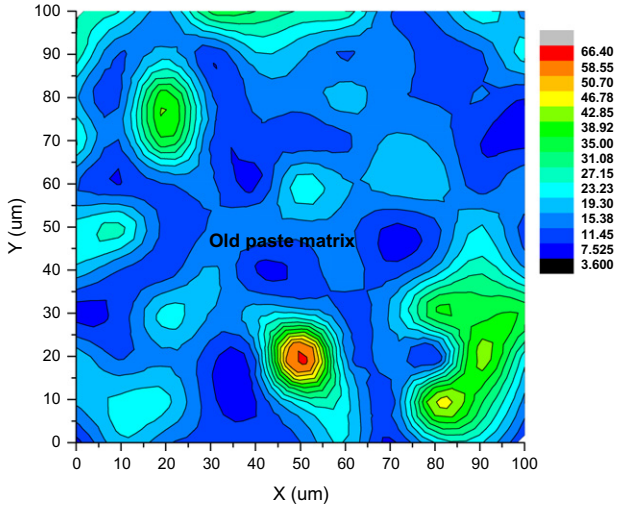


(c) Contour map of indentation modulus in GPa

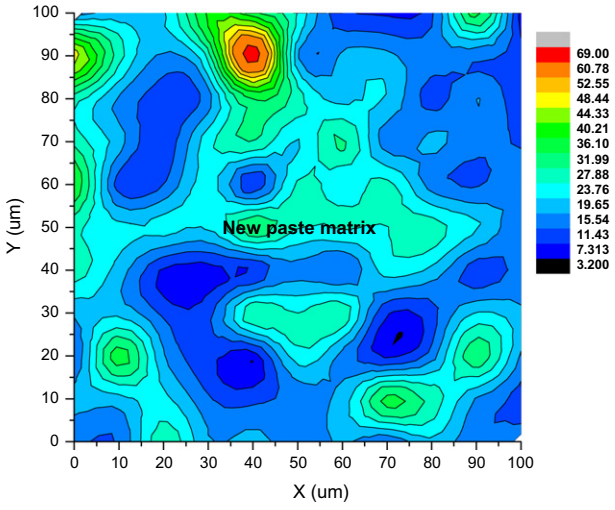


(d) Contour map of indentation modulus in GPa

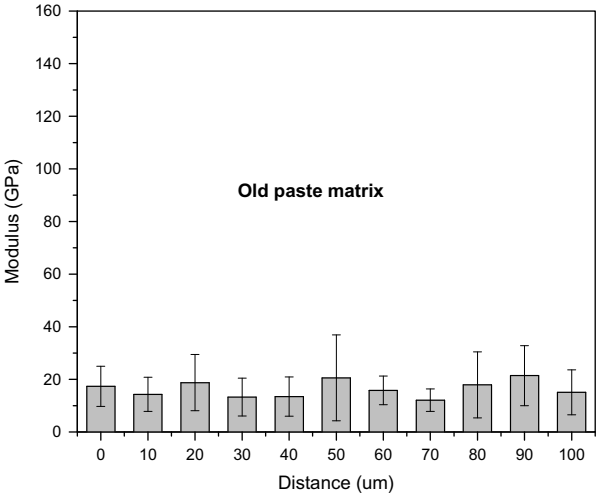


(e) Modulus in old paste matrix

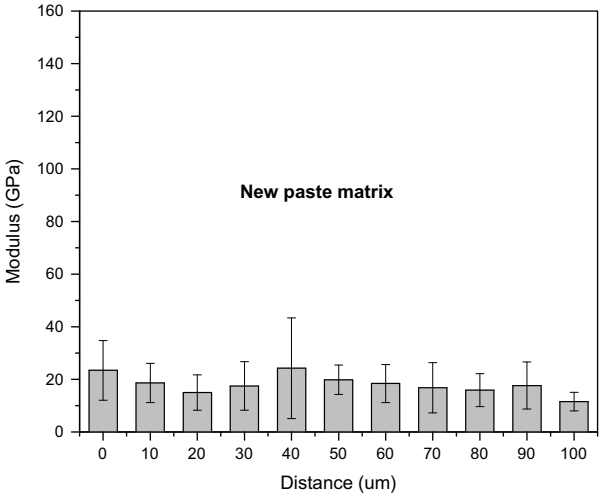


(f) Modulus in new paste matrix

**Fig. 12.** Indentation modulus in old and new paste matrices in RAC I at 90 days.

modulus. The thicknesses of old ITZ and new ITZ obtained from the hardness distribution (Fig. 9c and d) were also in a good agreement with that from the modulus distribution (Fig. 8e and f). On the other hand, the indentation hardness of old ITZ was found to be roughly 85% of that of old paste matrix, while the indentation hardness of new ITZ was found to be 90% that of new paste matrix. As the indentation hardness characteristics at old and new ITZs appeared to generally be similar to the indentation modulus characteristics, this

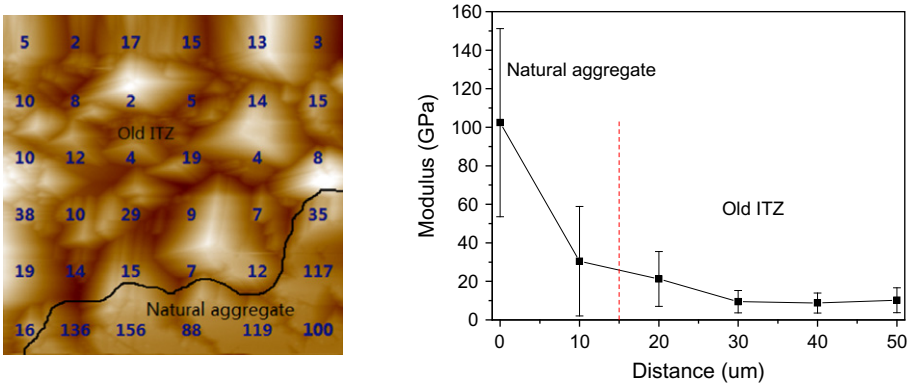


(a) Modulus on each location (60×60μm) (b) Modulus distribution across old ITZ

**Fig. 13.** Imaging indentation on old ITZ of RAC I at 90 days.

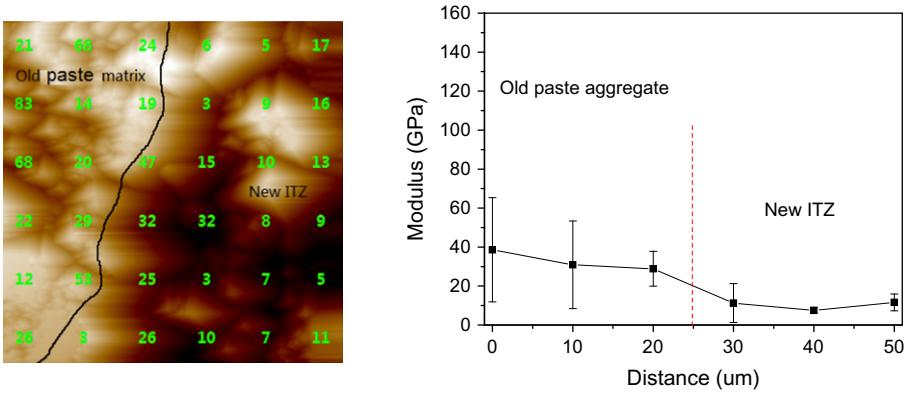


(a) Modulus on each location (60×60μm) (b) Modulus distribution across new ITZ

**Fig. 14.** Imaging indentation on new ITZ of RAC I at 90 days.

study will mainly discuss the indentation modulus in the following sections.

This SEM images provides evidence that the ITZs in RAC I at 90 days have different microstructure characteristics than the paste matrix. It can be observed that there are voids and calcium hydroxide (CH) crystals in the ITZs, especially perpendicular to old ITZ on the old paste matrix side. In comparison with old ITZ, there are more C–S–H gels existing at new ITZ (Fig. 10).

The SEM micrographs of polished sample with respect to microstructure in RAC I at 90 days are presented in Fig. 11. It shows that heterogeneities of the microstructure exist in both old and new ITZs. It can be seen clearly that higher porosity appears in old and new ITZ compared to the corresponding paste matrix. A comparatively denser zone close to new ITZ was found at the old paste aggregate side. It can be seen that interactions at new ITZ is considered to contribute to reduce the high porosity and improve the properties of the old paste aggregate perpendicular to new ITZ [12]. The denser zone around the paste aggregate surface is probably due to the further hydration process of the old paste matrix in vicinity of the new ITZ.

### 4.3. Grid nanoindentation on paste matrix

With the RAC I samples, nanoindentation was also performed at old paste matrix and new paste matrix (Fig. 12a and b). The chosen areas for indentation for both old and new paste matrix were 100 × 100 μm. And the spacing between indents is 10 μm in both lateral and vertical directions. Fig. 12c and d shows the contour map of indentation modulus at old paste matrix and new paste matrix, respectively. Some deep blue and black areas represented the relatively weak parts, such as voids and cracks. The red areas with maximum modulus typically represent the unhydrated cement particles [19]. Fig. 12e and f shows no obvious weak zones have been found in both old and new paste matrices. In comparison, the average indentation modulus of new paste matrix is slightly higher than that of the old paste matrix. This result is probably due to the different mix proportions that used when casting original concrete and the recycled concrete. But for the original concrete, the mix proportion record is usually difficult to obtain.

### 4.4. Imaging nanoindentation

Hundreds of indentations can be performed on a grid to generate enough data without any bias for a statistical analysis. However, grid indentation occasionally misses some positions of specific interest for the statistical analysis. On the other hand, imaging indentation becomes preferred when the nanomechanical properties of a local area on the sample are focused on. The image capability of the Triboindenter can also provide an effective method to examine the different phases in RAC. Fig. 13a is a 60 × 60 μm Scanning Probe Microscopy (SPM) image of the old ITZ in RAC I with the indentation modulus written on each point. The bright area near the right bottom of the image represents the old natural aggregate. There are areas very close to the natural aggregate that seems softener and more porous. Thirty six indents were performed on selected points. The spacing between these indented

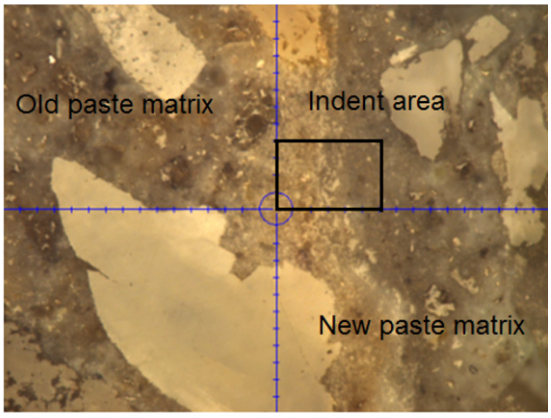


(a) New ITZ, indent area:150×100μm

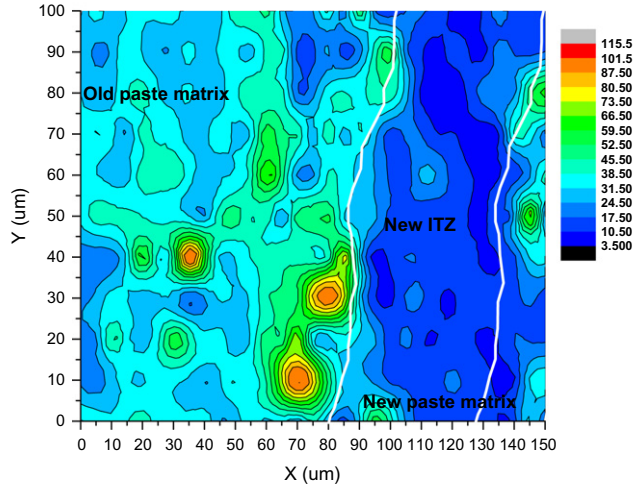


(b) Contour map of modulus in GPa

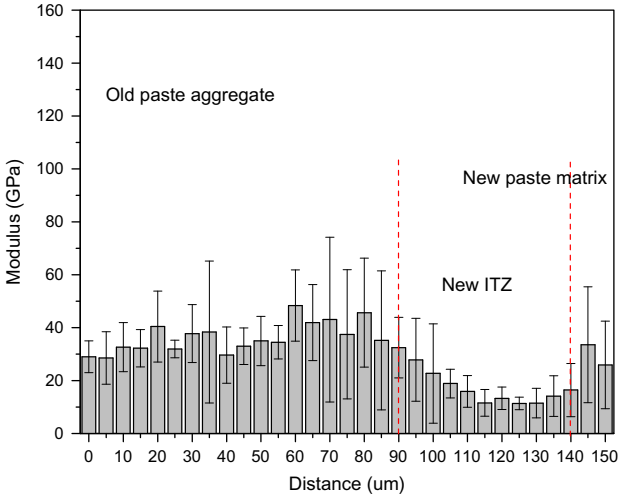


(c) Modulus distribution across new ITZ

**Fig. 15.** Grid indentation across new ITZ in RAC II at 90 days.

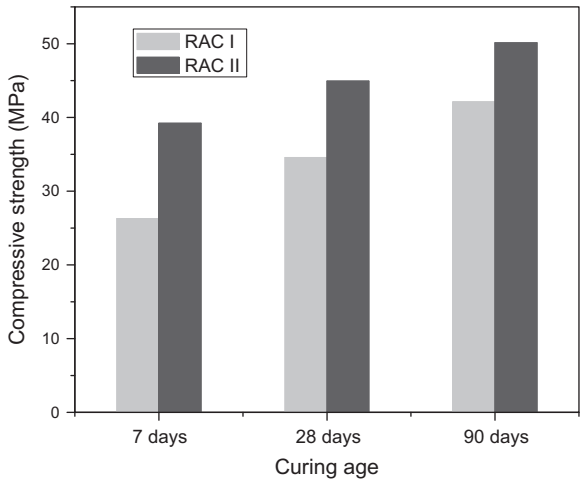


**Fig. 16.** Compressive strength development of RAC I and RAC II.

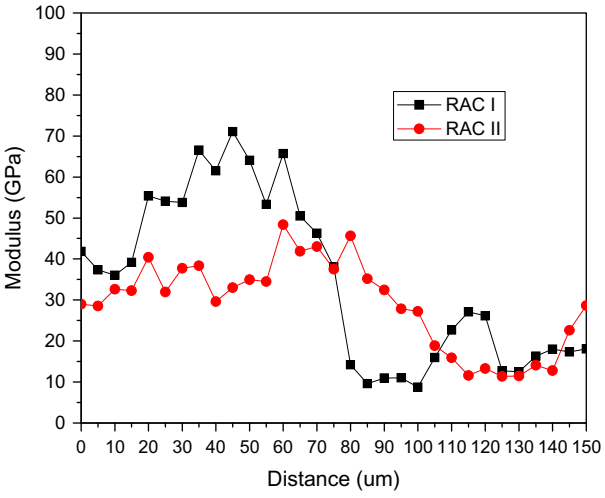


**Fig. 17.** Modulus distribution across new ITZ of RAC I and RAC II.

points was 10 μm. It can be figured out that at the extreme vicinity of the natural aggregate, the old ITZ generally has a lower modulus (ranged from 2 to 9 GPa). It should be noted that the connectivity of the weaker areas such as large voids and cracks along the interface influences the mechanical properties of RAC. Fig. 13b shows that the relatively lower modulus in the vicinity of natural aggregate (around 20–30 μm from the aggregate surface) has been measured within the old ITZ. It shows that extreme heterogeneity and poor nanomechanical properties exist in old ITZ.

Higher resolution SPM image with the indentation modulus value obtained from each location shows some pores existing in the new ITZ (Fig. 14a). Indentation was performed on 36 selected points. It is observed that the new ITZ has higher porosity in the vicinity of old paste aggregate (dark areas in the figure). The modulus of the areas with large voids ranges from 3 to 9 GPa. It is also seen that the relatively lower modulus of new ITZ exists at the vicinity of old paste aggregate (around 10–20 μm from the old paste aggregate surface), but no trend of increasing modulus with distance moving away from the old paste matrix surface was found (Fig. 14b). This can tell that new ITZ itself is not a uniform region and the vicinity of new interface at the old paste aggregate side is a weak part within the new ITZ region.

## 5. Comparisons and discussions

### 5.1. Effect of mix proportion on new ITZ

Similar nanoindentation test was undertaken on RAC II also at 90 days old. Figs. 8b and 15a show the indent location of new ITZ

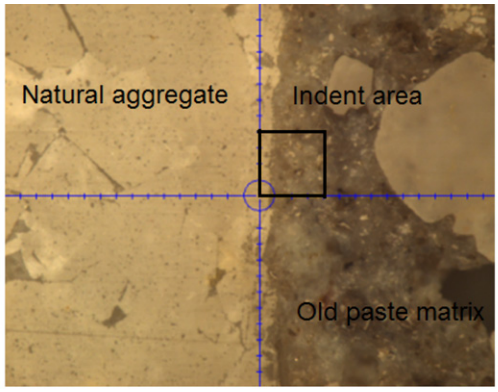


(a) Old ITZ around limestone: 100×100 μm

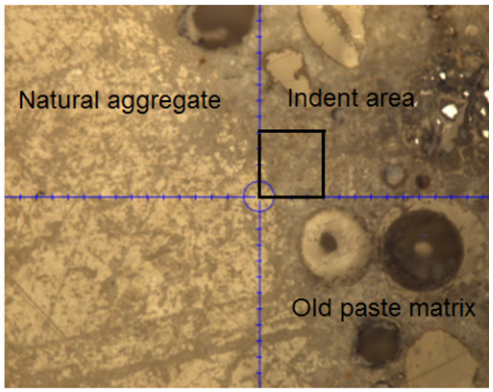


(b) Old ITZ around gravel: 100×100 μm

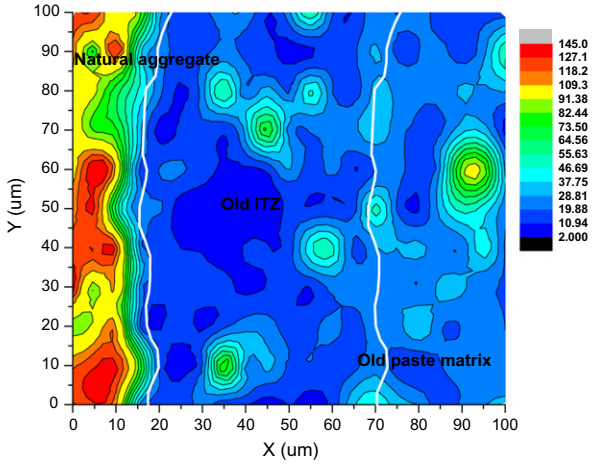


(c) Contour map of modulus in GPa (old ITZ)

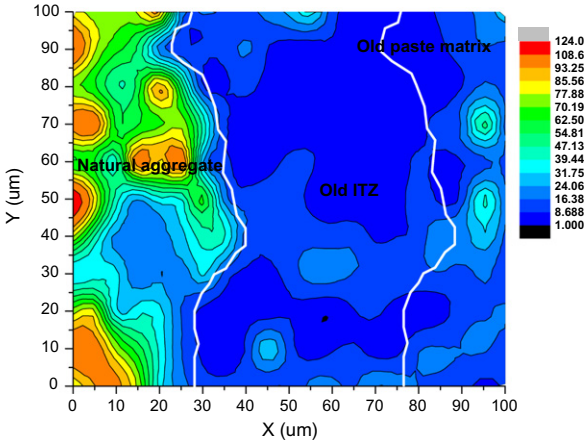


(d) Contour map of modulus in GPa (old ITZ)

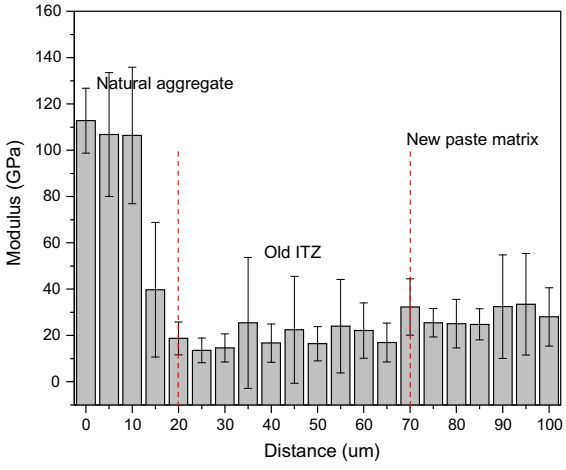


(e) Modulus distribution across old ITZ

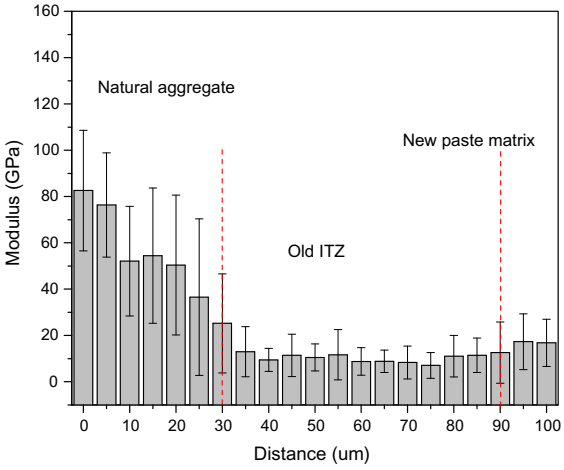


(f) Modulus distribution across old ITZ

**Fig. 18.** Grid indentation across old ITZ around different aggregates in RAC I at 90 days.

**Table 3**
Characteristics of old ITZ and new ITZ in RAC (mean ± standard deviation).

| Items | | Old ITZ | | New ITZ | |
|---|---|---|---|---|---|
| | | Thickness (μm) | Modulus ratio ($M_{OITZ}/M_{OCP}$) (%) | Thickness (μm) | Modulus ratio ($M_{NITZ}/M_{NCP}$) (%) |
| Curing age (RAC I) | 7 days | 43 ± 10 | 77 ± 8 | 86 ± 9 | 97 ± 8 |
| | 28 days | 45 ± 12 | 81 ± 12 | 67 ± 15 | 91 ± 12 |
| | 90 days | 49 ± 11 | 84 ± 11 | 53 ± 20 | 84 ± 15 |
| Natural aggregate (RAC II at 90 days) | Limestone | 47 ± 18 | 82 ± 15 | – | – |
| | Gravel | 63 ± 5 | 71 ± 10 | – | – |

*Note*: $M_{OITZ}$: indentation modulus of old ITZ; $M_{OCP}$: indentation modulus of old paste matrix; $M_{NITZ}$: indentation modulus of new ITZ; $M_{NCP}$: indentation modulus of new paste matrix.

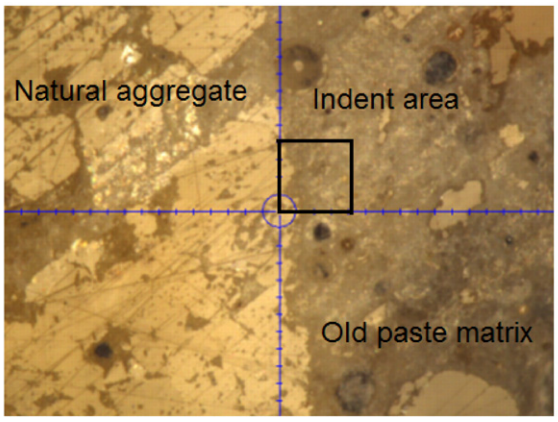


(a) Old ITZ, indent area:100×100μm

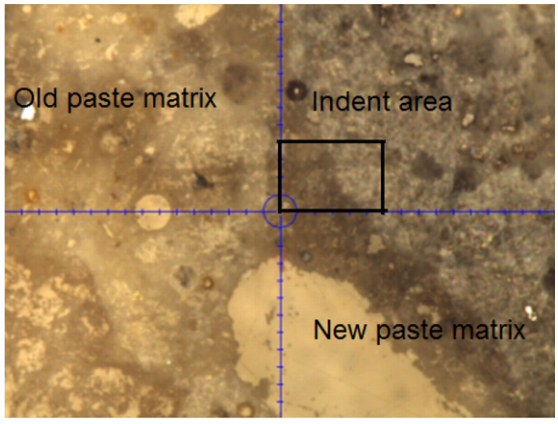


(b) New ITZ, indent area:150×100μm

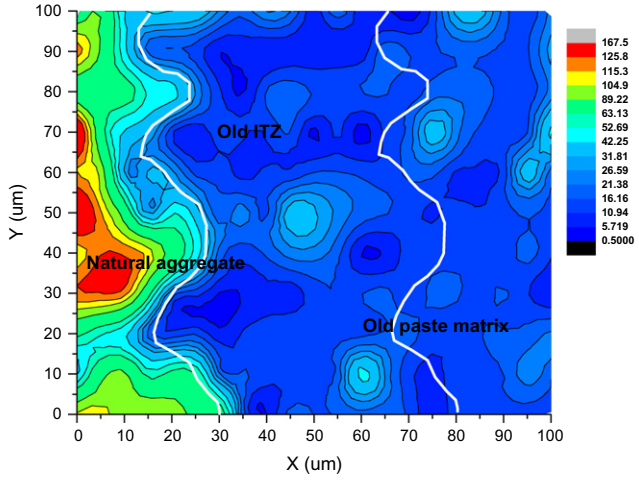


(c) Contour map of modulus in GPa (old ITZ)

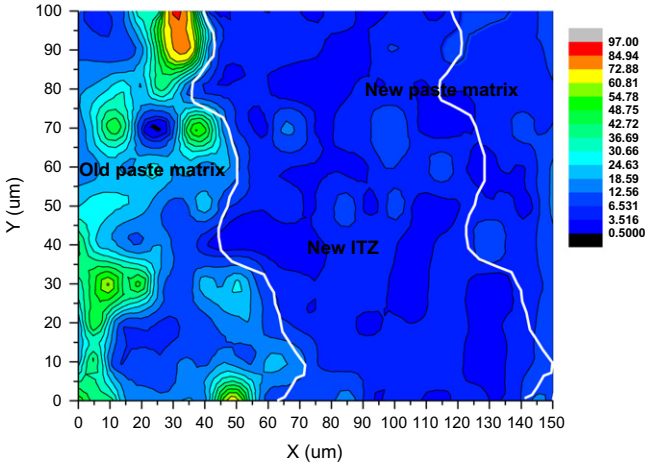


(d) Contour map of modulus in GPa (new ITZ)

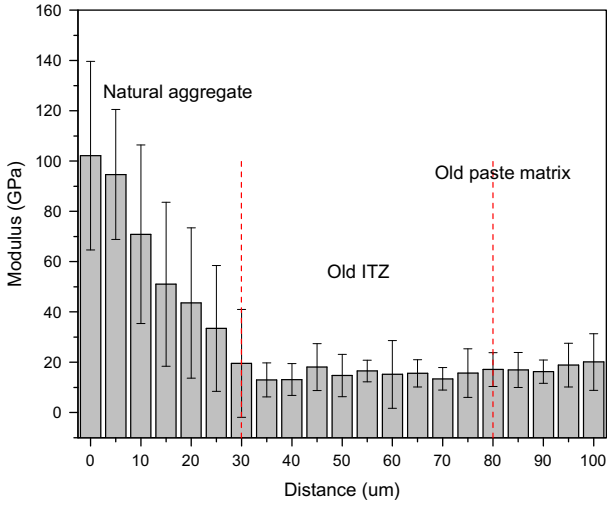


(e) Modulus distribution across old ITZ

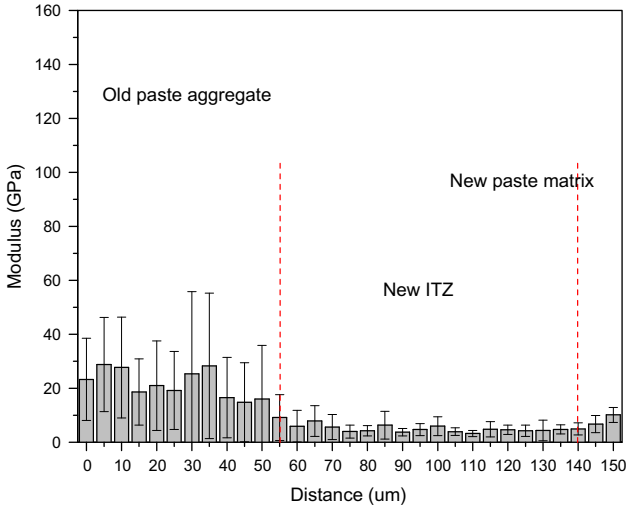


(f) Modulus distribution across new ITZ

**Fig. 19.** Grid indentation across ITZs of RAC II at 7 days.

in RAC I and RAC II, respectively. It exhibits that the indentation modulus of the old paste matrix close to new ITZ on the old paste aggregate side was higher compared to other regions in both RAC I and RAC II (Figs. 8d and 15b). Figs. 8f and 15c also show the indentation modulus distribution with the distance across the new ITZs. For the new ITZ in RAC I, the average indentation modulus is found to be around 85% of that of the new paste matrix. Similarly, the average modulus of new ITZ in RAC II is also found to be approximately 85% of that of new paste matrix. However, the average indentation modulus of new ITZ in RAC I is slightly lower than that

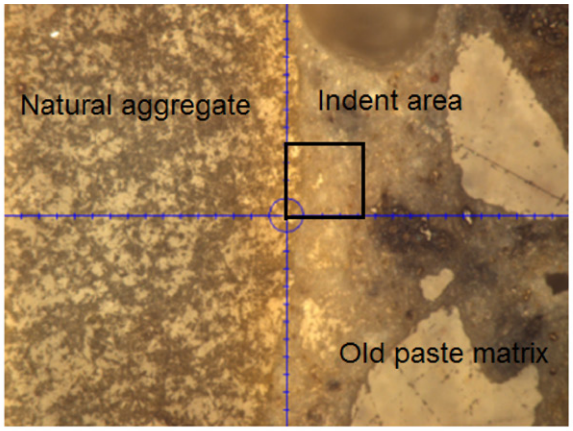


(a) Old ITZ, indent area:100×100μm

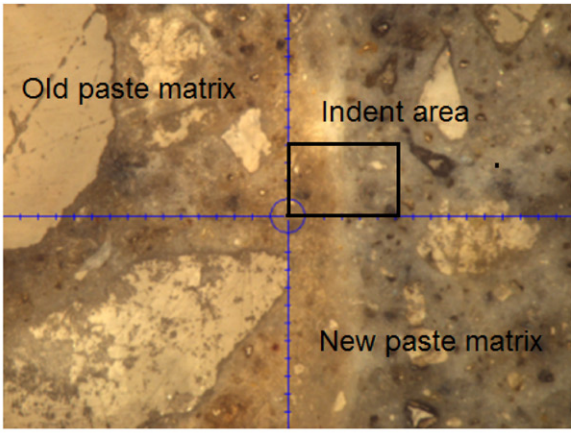


(b) New ITZ, indent area:150×100μm

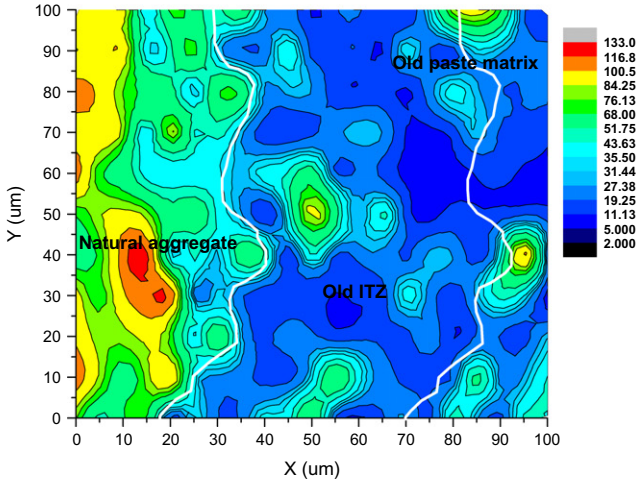


(c) Contour map of modulus in GPa (old ITZ)

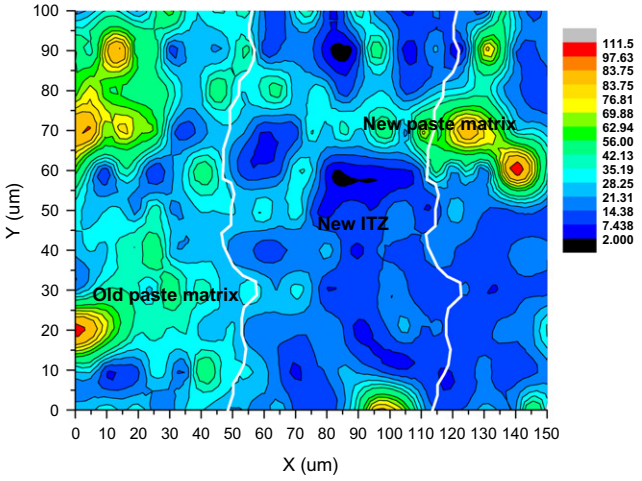


(d) Contour map of modulus in GPa (new ITZ)

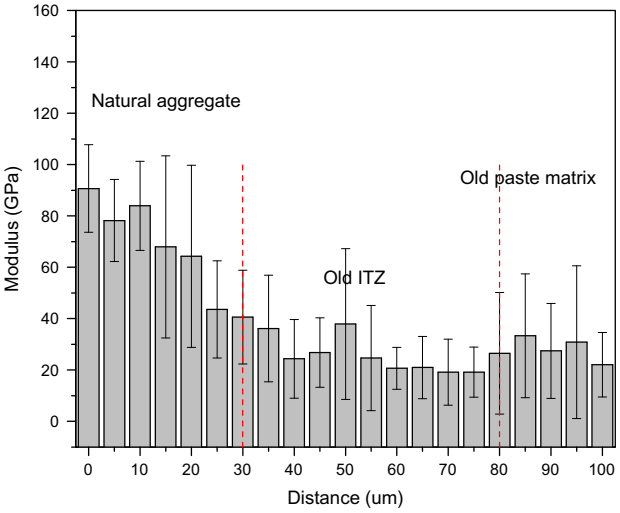


(e) Modulus distribution across old ITZ

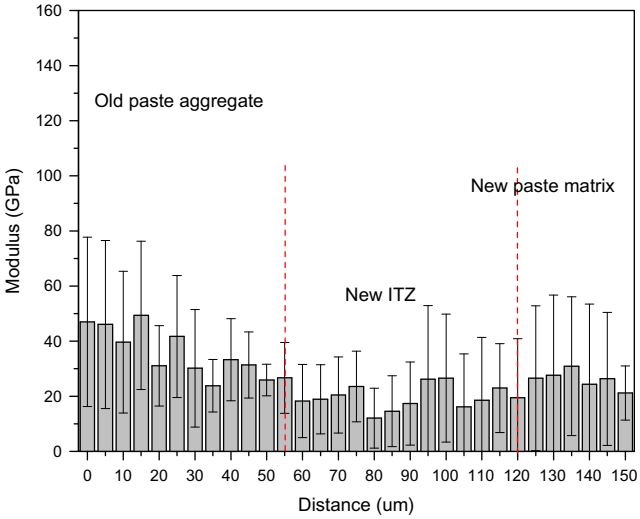


(f) Modulus distribution across new ITZ

**Fig. 20.** Grid indentation across ITZs in RAC II at 28 days.

of new ITZ in RAC II, even though the water-to-binder ratio used in RAC I was slighter lower. This can be attributed to the usage of fly ash in RAC I, as it is widely accepted that although fly ash can introduce pozzonlanic reactions to improve paste properties, it may also delay the hydration process.

To study the effect of mix proportion (fly ash) on the properties of the ITZs in RAC, the cylinder compressive strengths of RAC I and RAC II were also tested at 7, 28 and 90 days. Fig. 16 shows that the compressive strength of RAC I is lower than that of RAC II, while the strength development rate of RAC I is higher than that of RAC

II after 7 days. This corresponds to the finding that the new ITZ in RAC I is relatively weaker than that of new ITZ in RAC II and the thickness of new ITZ in RAC I is somewhat greater than that of new ITZ in RAC II (Fig. 17). Therefore, the nanomechanical properties of new ITZ can be used to explain the difference in strength between RAC I and RAC II. It can be induced that the compressive strength development of RAC are related to the nanomechanical properties of new ITZ.

### 5.2. Old ITZs around different types of aggregates

Fig. 18a and b shows the indent location of old ITZs around two types of natural aggregates (limestone and gravel) with similar sizes in RAC I at 90 days. For old ITZ around limestone aggregate, the thickness appeared to be around 50 μm. The average indentation modulus in old ITZ appeared to be around 80% of that of old paste matrix (Fig. 18c). As for the old ITZ around gravel, the thickness appeared to be 60 μm, which is more than that of old ITZ around limestone aggregate. This may be due to limestone normally having a rough surface and being more porous compared with gravel (Fig. 18d). The average indentation modulus of old ITZ around the gravel was observed to around 70% of that of the old paste matrix.

From Fig. 18e and f, it can be seen that the old ITZ around gravel aggregate achieved a lower indentation modulus than that of old ITZ around limestone, which is consistent with other investigations [40,41]. These results confirm that the properties of old ITZ in RAC appear to depend more on the original natural aggregate that used.

### 5.3. Age effect on ITZs

To study the hydration age effect on the ITZs in RAC, the RAC II samples were also studied by nanoindentation at 7, 28 and 90 days, respectively, as shown in Table 3. Fig. 19a and b shows the indent locations for old and new ITZs in RAC II at the age of 7 days. The contour maps of indentation modulus of old ITZ and new ITZ are shown in Fig. 19c and d, respectively. At 7 days age, both new ITZ and new paste matrix had relatively lower modulus than that of the old ITZ and the old paste matrix, correspondingly. There is no significant difference can be noticed between new ITZ and new paste matrix from Fig. 19d. The result suggests that new ITZ and new paste matrix are the weak links in RAC at an early age. At 7 days, the thickness of the old ITZ is found to be around 45 μm, which is consistent with that of old ITZ at later ages (Fig. 19e). Moreover, the modulus of the old ITZ was also estimated to be about 75% of old paste matrix, which was roughly the similar value with that of old ITZ at a later age. Therefore, the results can imply that the hydration age has no obvious effects on the nanomechanical properties of old ITZ. On the other hand, the indentation modulus of new ITZ was almost 95% of that of new paste matrix (Fig. 19f). The thickness of new ITZ is found to be approximately 85 μm, which indicates that the thickness of new ITZ at an early age is larger than the new ITZ at later ages. It can be concluded that the hydration age has a significant influence on the properties and development of new ITZ. This is mainly due to the further hydration in the new ITZs. With the hydration time increasing, the reduction of the porosity in new ITZ is initially because of the packing of anhydrous cement grains. Therefore, the thickness of new ITZ decreases with the hydration age increasing, and the new ITZ region becomes stronger and denser. Furthermore, the results show good agreements with previous studies that the properties of new ITZ are highly changed with the hydration process [29,42].

Fig. 20a and b shows the indent locations of ITZs in RAC II at 28 days. There was no significant difference in the indentation modulus of old ITZs between 7 days and 28 days of the sample based on the distribution of the indentation modulus (Fig. 20c). On the other hand, the indentation modulus of new ITZ and new paste matrix significantly increased at 28 days compared to that of 7 days age. However, the indentation modulus ratio of new ITZ to new paste matrix decreased. The relatively lower modulus in

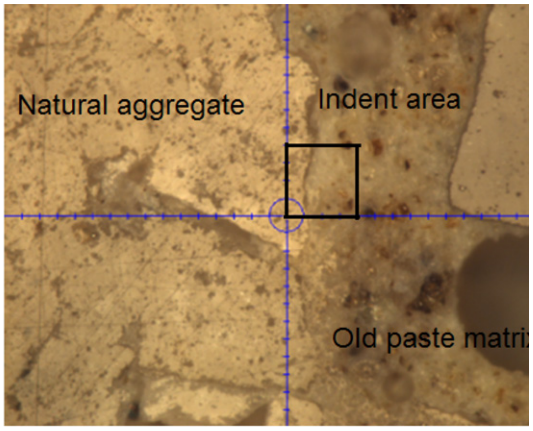


(a) Old ITZ, indent area:100×100μm

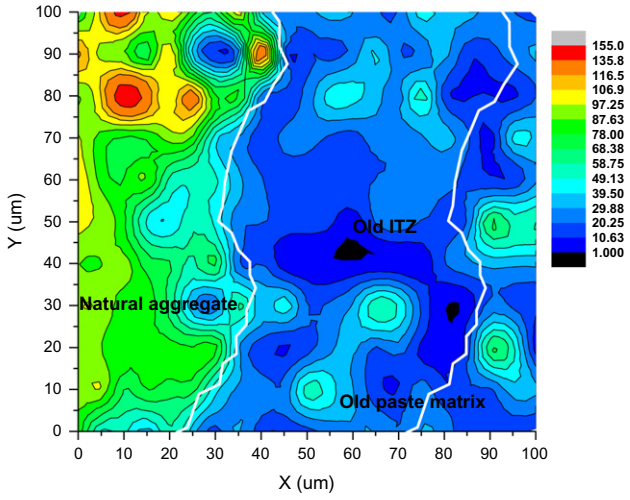


(b) Contour map of modulus in GPa (old ITZ)

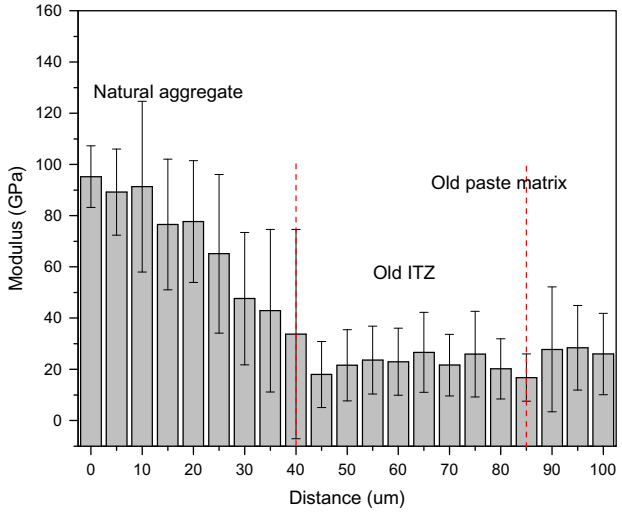


(c) Modulus distribution across old ITZ

**Fig. 21.** Grid indentation across old ITZs in RAC II at 90 days.

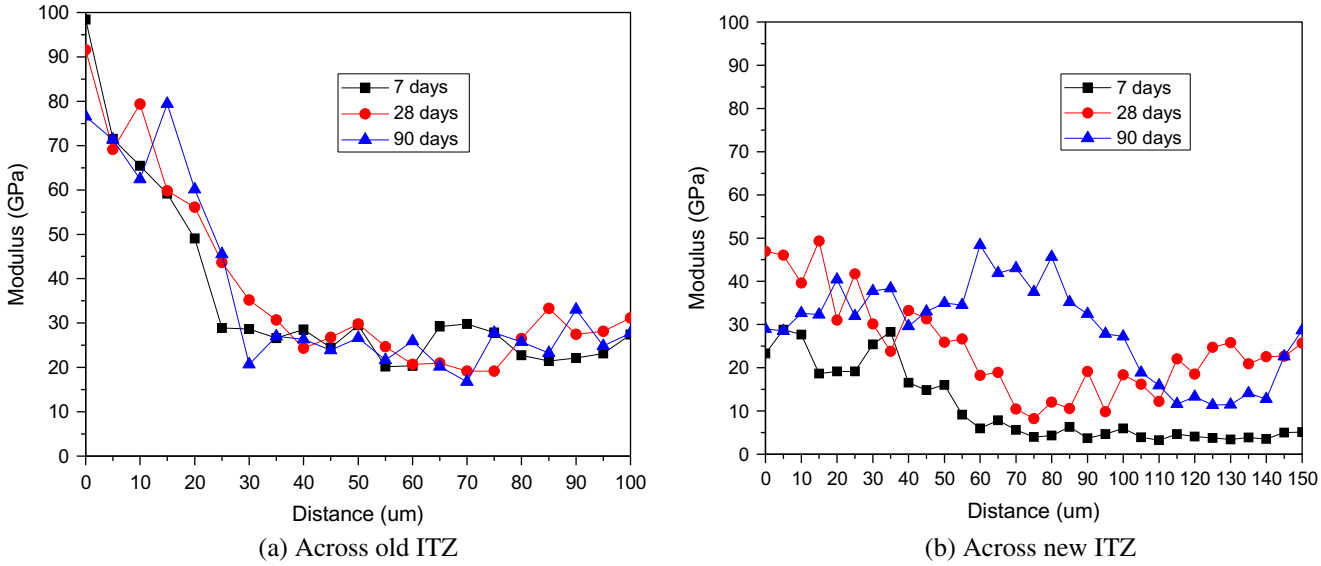


**Fig. 22.** Modulus distribution across ITZs of RAC II different hydration ages.

the new ITZ mostly occurred in the vicinity of the old paste aggregate at a distance 20 μm from the old paste matrix surface (Fig. 20d). As shown in Fig. 20e, the thickness of old ITZ was estimated to be around 50 μm, which was similar to that of old ITZ at 7 days age. The indentation modulus of old ITZ appeared to be around 80% of that of the old paste matrix. As for new ITZ, the average modulus was found to be approximately 90% of that new paste matrix (Fig. 20f). The thickness of new ITZ was considered to be around 65 μm, which was less than that of new ITZ at 7 days age. In comparison, the average indentation modulus of new ITZ was slightly lower than that of old ITZ in RAC II at 28 days age.

Figs. 21a and 15a show the indent location of ITZs in RAC II at 90 days. The old ITZ thickness still appeared to be around 50 μm. Indentation modulus in old ITZ appeared to be 85% of that of old paste matrix (Fig. 21b). There was no significant difference in the indentation modulus distribution of old ITZ among 7, 28 and 90 days hydration ages. This suggests that there are no further significant hydration progresses took place in the old ITZ during the testing period. As for the new paste matrix, the indentation modulus at 90 days was higher than that at 28 days as expected (Fig. 15b).

As shown in Fig. 21c, the modulus of old ITZ when RAC is 90 days old was almost similar with that of old ITZ in RAC at 7, 28 days age. As for new ITZ, the average modulus of new ITZ was found to be approximately 85% of that the new paste matrix (Fig. 17c). The thickness of new ITZ was considered to be around 55 μm, which was less than that of new ITZ in RAC at 28 days age. These results reveal that the thickness of new ITZ decreases with the hydration age.

The indentation modulus distributions of old and new ITZs in RAC II at 7, 28 and 90 days are compared and displayed in Fig. 22. It shows that the age effect on the indentation modulus of old ITZ and new ITZ in RAC was different. The properties of old ITZ in RAC do not change with the hydration age, while the indentation modulus of new ITZ and new paste matrix increases with the hydration age (Fig. 22a). At a late age, the indentation modulus increases at a lower rate compared to the early age (Fig. 22b). This trend is similar with that of the compressive strength development of RAC. It should be noted that the ratio between indentation modulus of new ITZ and new paste matrix decreases with the age.

## 6. Conclusions

Under the conditions and scopes of this experimental study, a number of conclusions for old and new ITZs in Recycled Aggregate Concrete (RAC) can be drawn in the following:

(1) This study developed successful protocols for grinding and polishing specimens and can achieve perfectly acceptable characterization of the surface roughness for nanoindentation, which was verified by AFM. From the SEM images, obvious voids and calcium hydroxide exist in both old and new ITZs in RAC.
(2) Based on the nanoindentation study, the thicknesses of old and new ITZs are found to be around 40–50 μm and 55–65 μm respectively at a late age. Moreover, the average modulus of old and new ITZs appears to be approximately 70–80% of that of old paste matrix and 80–90% of that of new paste matrix, respectively.
(3) From the imaging nanoindentation, for the old ITZ in RAC, the lowest modulus in the vicinity of aggregate is 20–30 μm from natural aggregate surface, while for the new ITZ, the lowest modulus of new ITZ existed in the vicinity of old paste matrix is 10–20 μm from the old paste aggregate surface.
(4) With the different types of natural aggregate, the indentation modulus of old ITZ around limestone is higher than that of old ITZ around gravel, and the thickness of old ITZ around limestone is thinner than that around gravel. However, both the mix proportion and hydration age have no obvious effects on the nanomechanical properties of the old ITZ in RAC.
(5) The average indentation modulus of new ITZ in RAC I was lower than that of new ITZ in RAC II, and the thickness of new ITZ in RAC I was greater than that in RAC II. This is probably attributed to the fly ash which was added in RAC I. With the increase of hydration age, the new ITZ thickness appears to be reduced and the microstructure at new ITZ tends to became denser because of the development of hydrates with the age.

## Acknowledgments

The authors would like to gratefully acknowledge the financial support from the National Natural Science Foundation of China

(51178340), and the Kwang-Hua Foundation. The authors gratefully thank Dr. Gajendra Shekhawat and Dr. David J. Corr in Northwestern University for their supports. The second author would also like to thank China Scholarship Council (CSC) for its partial financial support during his study at Northwestern University, USA.

## References

[1] ACI Committee 555. Removal and reuse of hardened concrete. ACI Mater J 2001;99(8):320–5.
[2] Xiao JZ, Li WG, Fan YH, Huang X. An overview of study on recycled aggregate concrete in China (1996–2011). Constr Build Mater 2012;31:364–83.
[3] Xiao JZ, Zhang Y, Cheung MS, Chu Reuben PK, editors. RILEM proceedings pro073: 2nd international conference on waste engineering and management – ICWEM 2010. Shanghai; 2010.
[4] Lange DA. Recycled concrete: the past, present and further. In: International symposium on environmental ecology and technology of concrete (EETC-2011), Beijing; 2011.
[5] Liu Q, Xiao JZ, Sun ZH. Experimental study on the failure mechanism of recycled concrete. Cement Concrete Res 2011;41(10):1050–7.
[6] Topcu IB, Sengel S. Properties of concretes produced with waste concrete aggregate. Cement Concr Res 2004;34(8):1307–12.
[7] Xiao JZ, Li WG, Poon CS. Recent studies on mechanical properties of recycled aggregate concrete in China – a review. Sci China: Technol Sci 2012;55: 1463–80.
[8] Poon CS, Shui ZH, Lam L, Fok H, Kou SC. Influence of moisture states of natural and recycled aggregates on the slump and compressive strength of concrete. Cement Concr Res 2004;34(1):31–6.
[9] Otsuki N, Miyazato S, Yodsudjai W. Influence of recycled aggregate on interfacial transition zone, strength, chloride penetration and carbonation of concrete. J Mater Civil Eng 2003;15(5):443–51.
[10] Domingo A, Lázaro C, Gayarre FL, Serrano MA, López-Colina C. Long term deformations by creep and shrinkage in recycled aggregate concrete. Mater Struct 2010;43(8):1147–60.
[11] Etxeberria M, Vázquez E, Marí A. Microstructure analysis of hardened recycled aggregate concrete. Mag Concrete Res 2006;58(10):683–90.
[12] Poon CS, Shui ZH, Lam L. Effect of microstructure of ITZ on compressive strength of concrete prepared with recycled aggregates. Constr Build Mater 2004;18(6):461–8.
[13] Xiao JZ, Li WG, Sun ZH, Shah SP. Crack propagation in recycled aggregate concrete under uniaxial compressive loading. ACI Mater J 2012;109(4): 451–61.
[14] Nagataki S, Gokce A, Saeki T, Hisada M. Assessment of recycling process induced damage sensitivity of recycled concrete aggregates. Cement Concrete Res 2004;34(6):965–71.
[15] Li WG, Xiao JZ, Sun ZH, Shah SP. Failure processes of modeled recycled aggregate concrete under uniaxial compression. Cement Concrete Comp 2012;34(10):1149–58.
[16] Li WG, Xiao JZ, Sun ZH, Kawashima S, Shah SP. Interfacial transition zones in recycled aggregate concrete with different mixing approaches. Constr Build Mater 2012;35:1045–55.
[17] Sorelli L, Constantinides G, Ulm F, Toutlemonde F. The nano-mechanical signature of ultra high performance concrete by statistical nanoindentation techniques. Cement Concrete Res 2008;38(12):1447–56.
[18] Sakulich AR, Li VC. Nanoscale characterization of engineered cementitious composites (ECCs). Cement Concrete Res 2011;41(2):169–75.
[19] Mondal P, Shah SP, Marks LD. Nanoscale characterization of cementitious materials. ACI Mater J 2008;105(2):174–9.
[20] Tarefder RA, Zaman AM, Uddin W. Determining hardness and elastic modulus of asphalt by nanoindentation. Int J Geomech 2010;10(3):106–16.
[21] Mondal P, Shah SP, Marks L. A reliable technique to determine the local mechanical properties at the nanoscale for cementitious materials. Cement Concrete Res 2007;37(10):1440–4.
[22] Davydov D, Jirásek M, Kopecký L. Critical aspects of nano-indentation technique in application to hardened paste matrix. Cement Concrete Res 2011;41(1):20–9.
[23] Oliver WC, Pharr GM. Improved technique for determining hardness and elastic modulus using load and displacement sensing indentation experiments. J Mater Res 1992;7(6):1564–83.
[24] Fischer-Cripps, Anthony C. Nanoindentation. New York: Springer; 2002.
[25] Miller M, Bobko C, Vandamme M, Ulm F-J. Surface roughness criteria for paste matrix nanoindentation. Cement Concrete Res 2008;38(4):467–76.
[26] Peled A, Castro J, Weiss J. Atomic force microscopy examinations of mortar made by using water-filled lightweight aggregate. J Transport Res Board 2010;2141:92–101.
[27] Tam VWY, Gao XF, Tam CM. Microstructural analysis of recycled aggregate concrete produced from two-stage mixing approach. Cement Concrete Res 2005;35(6):1195–203.
[28] Stutzman PE. Scanning electron microscopy in concrete petrography. In: Materials science of concrete special volume, proceedings November 1–3; 2001. p. 59–72.
[29] Maso JC. Interfacial transition zone in concrete. RILEM report of technical committee 108-ICC interfaces in cementitious composites. London: E&FN SPON; 1996.
[30] Elsharief A, Cohen MD, Olek J. Influence of aggregate size, water cement ratio and age on the microstructure of the interfacial transition zone. Cement Concrete Res 2003;33(11):1837–49.
[31] Tasong WA, Lynsdale CJ, Cripp JC. Aggregate-paste matrix interface. Part I. Influence of aggregate geochemistry. Cement Concrete Res 1999;29(7): 1019–25.
[32] Scrivener KL, Bentur A, Pratt PL. Quantitative characterization of the transition zone in high strength concrete. Adv Cem Res 1998;1(4):230–7.
[33] Crumbie AK. Characterisation of the microstructure of concrete. PhD Thesis, University of London; 1994.
[34] Jeong H. Processing and properties of recycled aggregate concrete. Master thesis, University of Illinois at Urbana-Champaign, Urbana, IL; 2011.
[35] Tam VWY, Tam CM. Assessment of durability of recycled aggregate concrete produced by two-stage mixing approach. J Mater Sci 2007; 42(10):3592–602.
[36] Kjellsen KO, Monsøy A, Isachsen K, Detwiler RJ. Preparation of flat-polished specimens for SEM-backscattered electron imaging and X-ray microanalysis-importance of epoxy impregnation. Cement Concrete Res 2003;33(4):611–6.
[37] Němeček J. Creep effects in nanoindentation of hydrated phases of cement pastes. Mater Charact 2009;60(9):1028–34.
[38] Constantinides G, Ulm F-J. The effect of two types of C–S–H on the elasticity of cement-based materials: results from nanoindentation and micromechanical modeling. Cement Concrete Res 2004;34(1):67–80.
[39] Scrivener KL, Crumbie AK, Laugesen P. The interfacial transition zone (ITZ) between paste matrix and aggregate in concrete. Interf Sci 2004;12(4):411–21.
[40] Diamond S. Considerations in image analysis as applied to investigations of the ITZ in concrete. Cement Concrete Comp 2001;23(2–3):171–8.
[41] Mondal P, Shah SP, Marks LD. Nanomechanical properties of interfacial transition zone in concrete. Nanotech Constr 2009;3:315–20.
[42] Zampini D, Shah SP, Jennings HM. Early age microstructure of the paste-aggregate interface and its evolution. J Mater Res 1998;13(7):1888–98.